Available online at www.sciencedirect.com

ScienceDirect

Ceramics International 40 (2014) 3031–3039

CERAMICS INTERNATIONAL

www.elsevier.com/locate/ceramint

Effect of suspension medium on the electrophoretic deposition of hydroxyapatite nanoparticles and properties of obtained coatings

Morteza Farrokhi-Rad, Taghi Shahrabi*

Department of Materials Science & Engineering, Tarbiat Modares University, P.O. Box 14115-143, Tehran, Iran

Received 19 July 2013; received in revised form 24 September 2013; accepted 1 October 2013
Available online 11 October 2013

Abstract

The suspensions of hydroxyapatite (HA) nanoparticles were prepared in different alcohols. The zeta potential of HA nanoparticles was the highest in butanolic suspension (65.65 mV) due to the higher adsorption of $RCH_2OH_2^+$ species via hydrogen bonding with surface P–OH group of HA. Electrophoretic deposition was performed at 20 and 60 V/cm for different times. Deposition rate was faster in low molecular weight alcohols due to the higher electrophoretic mobility of HA nanoparticles in them. The coating deposited from butanolic suspension had the highest adhesion strength and corrosion resistance in SBF solution at 37.5 °C. The surface of this coating was covered by apatite after immersion in SBF solution for 1 week.

Keywords: C. Corrosion; Alcohol; Coating; Electrophoretic deposition (EPD); Hydroxyapatite (HA) nanoparticles

1. Introduction

Hydroxyapatite (HA) is the main inorganic part of human bone [1]. HA has good bioactivity, biocompatibility, osteoconductivity and biodegradability so that it has been extensively used in biomedical applications [2–4]. However, HA has poor mechanical properties (such as low facture toughness) limiting its orthopedic applications. So usually it is applied as the coating on the metallic implants such as titanium and stainless steel. Electrophoretic deposition (EPD) has been extensively used to deposit HA coatings on the metallic substrates [5–10]. EPD is a two step process: in the first step charged particles are dispersed in a suitable liquid and migrate towards the electrode with opposite charge under the application of electric field. In the second step, they deposit there and form a relatively dense layer of particles on it [11]. EPD has several advantages such as simplicity, need to low cost equipments, ability to manipulate the microstructure of deposit by the simple adjustment of process parameters such as deposition time, voltage and so on [11]. Due to the particulate nature of EPD it has the ability to deposit the coatings with interconnected porosity appropriate for implant fixation by bone ingrowths into them [12].

The kinetics of EPD follows from the Hamaker equation [13]

$$\frac{dw}{dt} = f\mu cAE \tag{1}$$

Where μ is the electrophoretic mobility of particles, c is the concentration of suspension, A is the deposition area and E is the applied electric field and f is a factor introduced into the equation to take into account that not all the particles brought to the substrate electrode take part in deposit formation. The electrophoretic mobility of particles can be obtained by the following equation [14]

$$\mu = \frac{\varepsilon_0 \varepsilon_r \zeta}{\eta} \tag{2}$$

Where ε_0 is the vacuum permittivity (8.854×10^{-12} F/m), ε_r is the relative dielectric constant of medium, ζ is the zeta potential of particles, and η is the viscosity of medium.

Using water as the suspension medium in EPD is limited due to its electrolysis at relatively low applied electric fields; the water electrolyses generates hydrogen and oxygen gases at cathode and anode, respectively, resulting in the deposits with

*Corresponding author. Tel.: +98 21 8288 3378; fax: +98 21 8288 3381.
E-mail addresses: morteza_farrokhi_rad@yahoo.com (M. Farrokhi-Rad), tshahrabi34@modares.ac.ird (T. Shahrabi).

0272-8842/$ - see front matter © 2013 Elsevier Ltd and Techna Group S.r.l. All rights reserved.
http://dx.doi.org/10.1016/j.ceramint.2013.10.004

poor quality microstructure including pin holes and bubbles [15]. So, non-aqueous solvents such as alcohols are usually used as the suspension medium in EPD [16,17]. In this work the EPD of HA nanoparticles from different alcoholic suspensions (methanol, ethanol, isopropanol and butanol) and the properties of obtained coatings have been investigated.

2. Materials and methods

2.1. Suspensions preparation

Hydroxyapatite (HA) nanoparticles were synthesized by metathesis method [18]. The suspensions of HA nanoparticles (10 g/L) were prepared in methanol (99.99%, Merck), ethanol (99.8%, Merck, Germany), isopropanol (99.9%, Merck, Germany) and butanol (99%, Merck, Germany) by the addition of 1 g HA nanoparticles into 100 mL of alcohols and magnetically stirring them for 24 h. Finally, the suspensions were ultrasonically dispersed for 10 min (Sonopuls HD 3200, 20 kHz; Bandelin Co., Berlin, Germany). The electrical conductivity of the alcohols was measured before and after the addition of 10 g/L HA nanoparticles into them with the accuracy of ± 0.01 μS/cm (Cond 720, WTW series; Inolab, Weilheim, Germany). The zeta potential of HA nanoparticles was measured in different alcoholic suspensions (Malvern instrument, 3000HS, Worcestershire, U.K). The FTIR analysis was used to investigate the adsorption of alcoholic molecules on the HA nanoparticles. The samples for FTIR analysis were prepared by the following method: some powders were extracted from the suspensions by centrifuging (6000 rpm, 15 min) then washed with deionized water (3 times) and dried at 100 °C for 24 h.

2.2. Electrophoretic deposition

Electrophoretic deposition (EPD) was performed using a two electrode cell. Both the working (substrate) and counter electrodes were the plates of 316 L stainless steel with the dimension of 20 mm × 10 mm × 1 mm. Only 10×10 mm^2 of substrates was exposed to deposition and remainder insulated. EPD was performed at 20 and 60 V/cm for different times (30, 120, 240, 360, 480 and 600 s) using a laboratory D.C. power supply (HY30002E; Huayi Electronics Industry Co., Hangzhou, Zhejiang, China). The current density during EPD was recorded by computer connected multimeter (289 True RMS; Fluke, Everett, WA). Deposition rate was studied by weighting the substrate before and after EPD using a 0.1 mg accuracy balance (GR-200; A&D Co., Tokyo, Japan). EPD was performed 3 times for each specimen and the average weight of deposition was calculated.

2.3. Coatings characterization

Deposits were dried at room temperature overnight. The thickness of dried coatings was measured by a coating thickness gauges (Qnix 8500, Germany). Thickness measurement was performed on the 3 specimen and the average

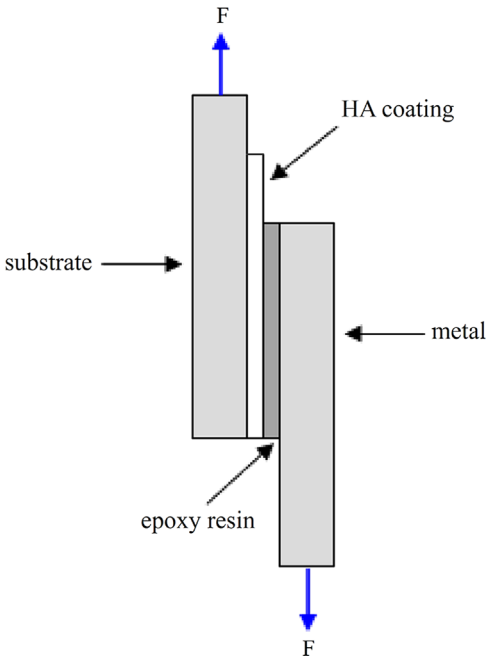

Fig. 1. Schematics of adhesion strength testing of HA coating on 316L stainless steel substrate.

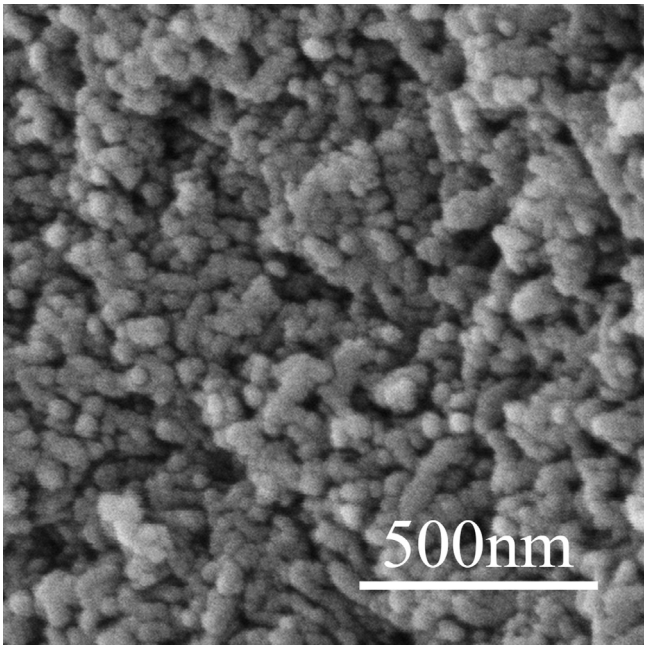

Fig. 2. SEM image of synthesized HA nanoparticles.

Table 1
The values of electrical conductivity of alcohols in the absence as well as the presence of 10 g/L HA nanoparticles.

Type of alcohol	Electrical conductivity (μS/cm)	
	Without HA	With 10 g/L HA nanopowder
Methanol	0.7	3
Ethanol	0.3	1.3
Isopropanol	0.2	0.16
Butanol	0.15	0.12

thickness was calculated. Deposits were sintered at 800 °C (heating rate: 5 °C/min) under flowing argon gas atmosphere (flow rate: 20 mL/min) for 1 h. The microstructure of the deposits was observed by scanning electron microscope (SEM) before and after their sintering. The adhesion strength of the coatings to the substrate was measured according to ASTM F1044-87, as shown in Fig. 1. The coatings were glued to 316 L stainless steel plates with the same dimension as the substrate using epoxy resin. The epoxy resin was cured in an oven at 100 °C for 2 h. The strength was measured by a universal testing machine. Three specimens were used in the adhesion tests and the average adhesion strength was calculated. The effect of HA coatings deposited at 20 V/cm for 60 s from different alcoholic suspensions on the corrosion resistance of 316L stainless steel in simulated body fluid (SBF) environment at 37.5 °C was studied by potentiodynamic polarization technique (Autolab 84367, Germany). SBF was prepared according to the method described in Ref. [19]. A three electrode cell was used for potentiodynamic polarization studies. Uncoated (bare substrate) and HA coated substrates were used as the working electrode. Saturated calomel electrode (SCE) and a platinum wire mesh were used as the reference and counter electrodes, respectively (scan rate: 1 mV/s). The bioactivity of the coatings was studied by their immersion in SBF solution at physiologic pH: 7.40 and temperature: 37.5 °C for 1 week. The ratio of coating surface area to SBF volume was fixed in 0.1 cm^{-1}. The specimens were taken out from SBF after 1 week, rinsed with deionized water, dried at room temperature overnight and their microstructure was observed by SEM.

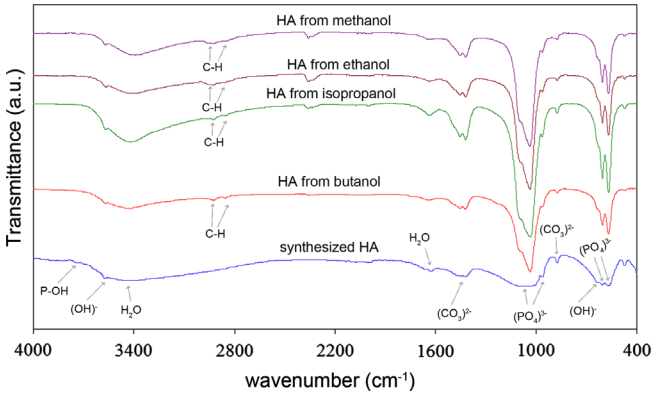

Fig. 3. FTIR spectra of synthesized HA nanopowder and HA nanopowder removed from different alcoholic suspension.

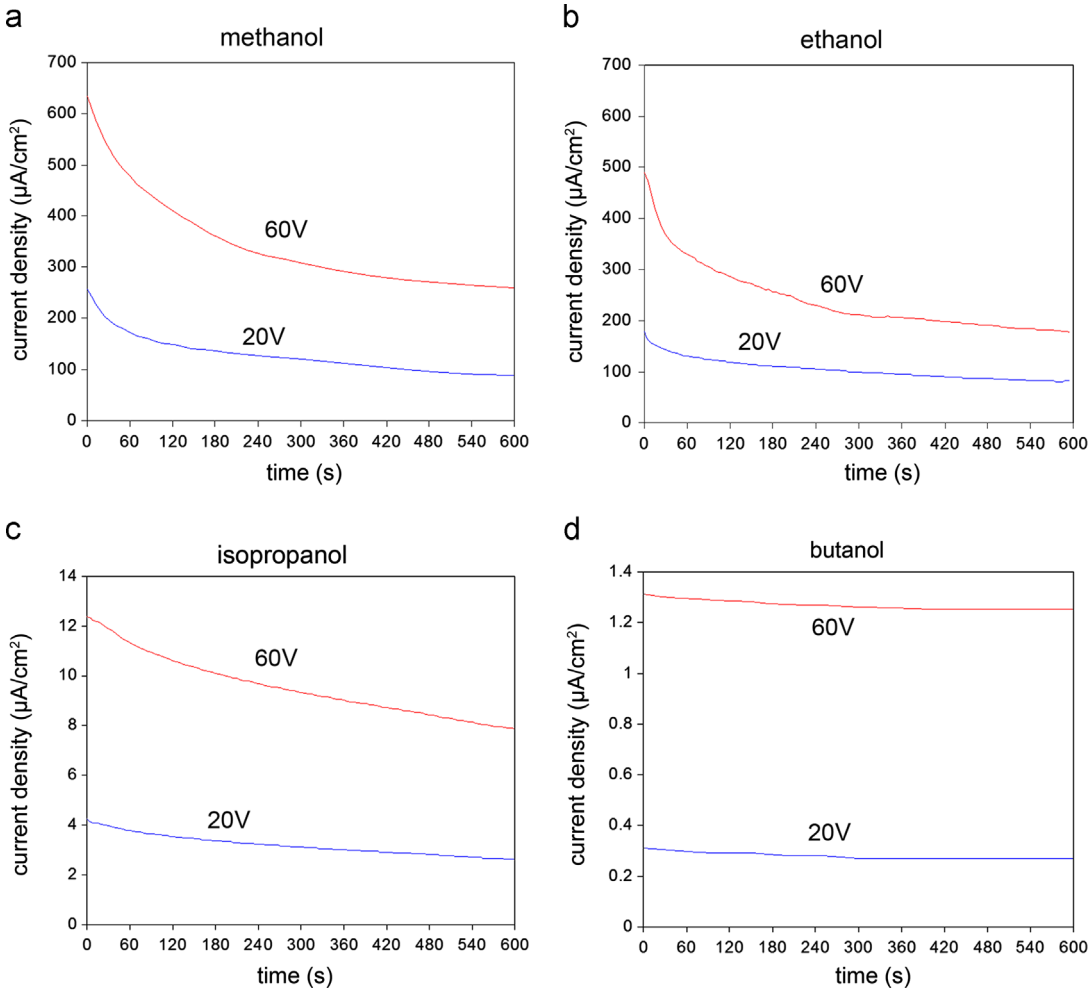

Fig. 4. Current density against deposition time at 20 and 60 V/cm from (a) methanolic (b) ethanolic (c) isopropanolic and (d) butanolic suspensions.

3. Results and discussion

3.1. Suspensions properties

The SEM micrograph of the synthesized HA nanoparticles are shown in Fig. 2. As can be seen in Fig. 2 particles have spherical morphology with the crystal size of about 30–50 nm. The electrical conductivity of the alcohols in the absence as well as the presence of HA nanoparticles (10 g/L) is listed in Table 1. As can be seen in Table 1 the electrical conductivity of methanol and ethanol increases upon the addition of 10 g/L HA nanoparticles into them, while that of isopropanol and butanol decreases. A pure alcohol can be ionized as follows [20]:

$$RCH_2OH + RCH_2OH = RCH2OH_2^+ + RCH2O^- \quad (3)$$

The tendency for this reaction decreases as the molecular weight of alcohol increases resulting in the lower conductivity for the alcohols with larger molecular size (the equilibrium constant for reaction (3) is $10^{-17.2}$, $10^{-18.88}$, $10^{-20.89}$ and $10^{-21.56}$ for methanol, ethanol, isopropanol and butanol, respectively [21]). The surface of HA nanoparticles can catalyze this reaction. $RCH_2OH_2^+$ species generated by reaction (3) can be adsorbed on the HA nanoparticles through hydrogen bonding with their surface P–OH groups (see Fig. 3). The measured values for the zeta potential of HA nanoparticles in methanol, ethanol, isopropanol and butanol are 27.67, 19.47, 38.17 and 65.65 mV, respectively. The adsorption of $RCH_2OH_2^+$ on the surface of HA nanoparticles results in the positive zeta potential for them. The zeta potential of HA nanoparticles in isopropanol (38.65 mV) and specially butanol (65.65 mV) is higher than that of those in methanol (27.67 mV) and ethanol (19.47 mV). The smaller the molecular size of alcohol the stronger the solvation interaction between it and $RCH_2OH_2^+$ species generated through reaction (3); so it is easier for $RCH_2OH_2^+$ species to release from the shield of larger molecular size alcohols and adsorb on the HA nanoparticles resulting in the more adsorption of $RCH_2OH_2^+$ species on the HA nanoparticles in isopropanol and butanol. The conductivity of isopropanol and butanol decreases when 10 g/L HA nanoparticles are added into them (Table 1) since the mobility of charged particles ($RCH_2OH_2^+$ adsorbed HA nanoparticles) is less than free $RCH_2OH_2^+$ ionic species.

The FTIR spectra of the synthesized HA nanopowders as well as that of those removed from different alcoholic suspensions are shown in Fig. 3. The bonds attributed to the peaks appeared in the FTIR spectra noted for each peak [22–24]. The peak at 3750 cm^{-1} belongs to the surface P–OH groups of HA

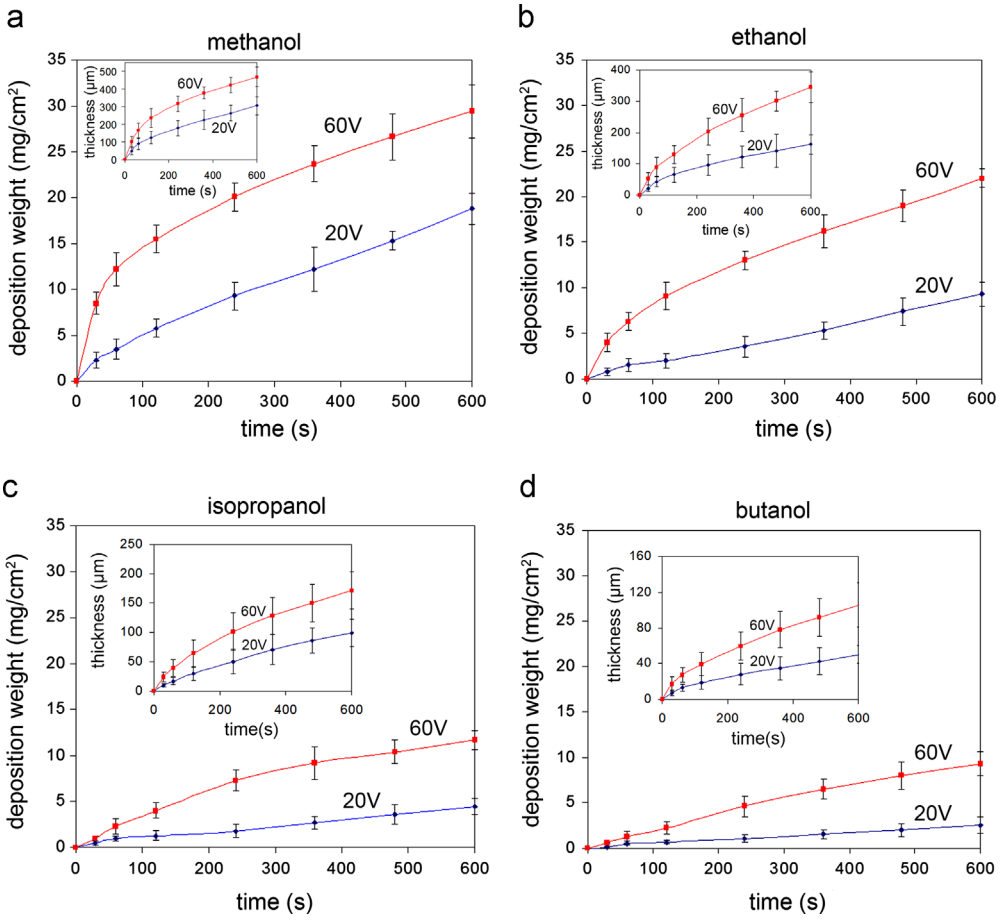

Fig. 5. Deposition weight against deposition time at 20 and 60 V/cm from (a) methanolic (b) ethanolic (c) isopropanolic and (d) butanolic suspensions. Inset figures show the thickness of coatings against time.

[25]. This peak disappears in the spectra of the powders removed from different alcoholic suspensions. While two other peaks are appeared at 2870 and 2940 cm^{-1} attributed to the stretching vibration of C–H bond. These results imply that alcohol molecules are adsorbed on the HA nanoparticles by hydrogen bonding with their surface P–OH groups. It has been reported that surface P–OH groups of HA can act as the preferred sites for the adsorption of H_2O, CO_2, CH_3OH, pyridine, n-butylamine, triethanolamine and acetic acid via hydrogen bonding [9,26,27].

3.2. Electrophoretic deposition

The current density curves against EPD time at 20 and 60 V/cm from different alcoholic suspensions are shown in Fig. 4. As can be seen the current density decreases with EPD time due to the formation of ceramic layer with higher resistivity than the suspension from which it deposits [28]. Current density deceases faster at 60 V/cm than 20 V/cm due to the faster growth of deposit at higher voltages. Also the reduction in current density in the case of butanolic suspension is lower due to the slower rate of deposition from it.

Fig. 5 shows the weight and thickness (inset figures) of the coatings against time for those deposited at 20 and 60 V/cm from different alcoholic suspensions. As can be seen the deposition is faster at 60 V/cm due to the faster migration of particles toward the substrate electrode in higher applied voltages (Eq. 1). The deposition rate increases in the order: butanolic, isopropanolic, ethanolic and methanolic suspensions, since the electrophoretic mobility of HA nanoparticles increases as the molecular weight of alcohol decreases. The values of electrophoretic mobility of HA nanoparticles calculated using Eq. (2) are 1.331, 0.481, 0.302 and 0.279 μm.cm/V s in methanol, ethanol, isopropanol and butanol, respectively.

3.3. Coatings characterization

Low magnification SEM images of the coatings deposited at 20 V/cm for 60 s from different alcoholic suspensions are shown in Fig. 6. As can be seen the cracking in the coatings decreases as the molecular weight of alcohol increases, so that cracking does not occur in the coating deposited from butanolic suspension. The cracking occurs due to the mechanical stresses exerted on the coating as the result of shrinkages induced during drying. The intensive cracking in the coatings deposited from suspensions with small molecule size alcohol is due to their higher shrinkage during drying resulting from their larger thickness (the thickness is 89 ± 31, 43 ± 16, 17 ± 6 and 13 ± 4 μm for coatings deposited from methanolic, ethanolic, isopropanolic and butanolic suspensions, respectively).

The vapor pressure of alcohol increases as its molecular size decreases; the boiling point is 64.7, 78.4, 82.5 and 118 °C for

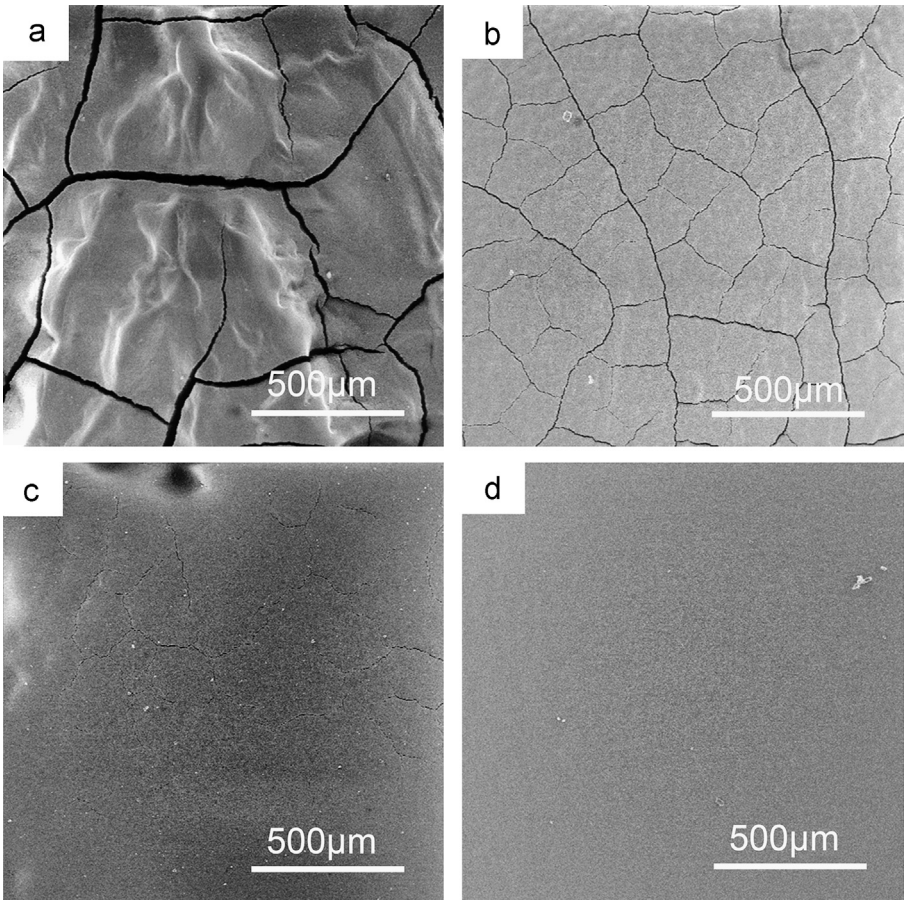

Fig. 6. Low magnification SEM images of coatings deposited at 20 V/cm and 60 s from (a) methanolic (b) ethanolic (c) isopropanolic and (d) butanolic suspensions.

methanol ethanol, isopropanol and butanol, respectively. Higher vapor pressure results in faster drying and possibly more cracking for the coatings deposited from small molecular size alcohols.

High magnification SEM images of the unsintered coatings deposited at 20 V/cm for 60 s from different alcoholic suspensions are shown in Fig. 7. As can be seen among the coatings the ones deposited from isopropanolic and especially butanolic suspensions have finer and more close packed microstructures. While those deposited from methanolic and ethanolic suspensions have agglomerated microstructure with the disordered arrangement of particles within them. The high quality microstructure of the coatings deposited from isopropanolic and butanolic suspensions is due to the higher zeta potential of HA nanoparticles (38.17 and 65.65 mV in isopropanoic and butanolic suspensions, respectively) as well as the slower kinetics of deposition (due to lower mobility) in them. The slower the kinetics of deposition the longer the time that particles find to sit in their best position to form a close packed microstructure. Higher electrophoretic mobility and lower zeta potential result in the poor quality of coatings deposited from methanolic and ethanolic suspensions.

The values for the adhesion strength of the coatings deposited at 20 V/cm for 60 s from methanolic, ethanolic, propanolic and butanolic suspensions are 5.5 ± 3.7, 7.3 ± 4.2, 10.5 ± 4.4 and 12.3 ± 4.7 MPa, respectively. As it was explained previously (Fig. 7) the coatings deposited from propanolic and butanolic suspensions have finer and more closely packed microstructures resulting in their good sinterability and so higher adhesion strength after sintering. The SEM images of the sintered deposits are shown in Fig. 8. As can be seen the coatings deposited from propanolic and butanolic suspensions have finer and more closely packed microstructure with less agglomerates.

The polarization curves for bare stainless steel substrate and substrates coated with HA at 20 V/cm for 60 s from different alcoholic suspensions are shown in Fig. 9. The values of corrosion potential (E_{corr}) and current density (i_{corr}) extracted from these curves are summarized in Table 2. Among the samples the one coated from butanolic suspension has the highest E_{corr} (-168 mV) and the lowest i_{corr} (0.58 μA/cm^2) and so the best corrosion resistance. This is due to the fine, dense and crack free microstructure of the coating deposited from butanolic suspension acting as the effective physical barrier against the corrosive SBF environment. There is some small cracks in the coating deposited from isopropanolic suspension (Fig. 6c) resulting in its lower corrosion protection efficiency. The coatings deposited from methanolic and ethanolic suspensions have very small corrosion protection efficiency due to their highly cracked microstructures. The cracks act as the diffusion path for corrosive SBF solution to reach the bare metal surface resulting in its

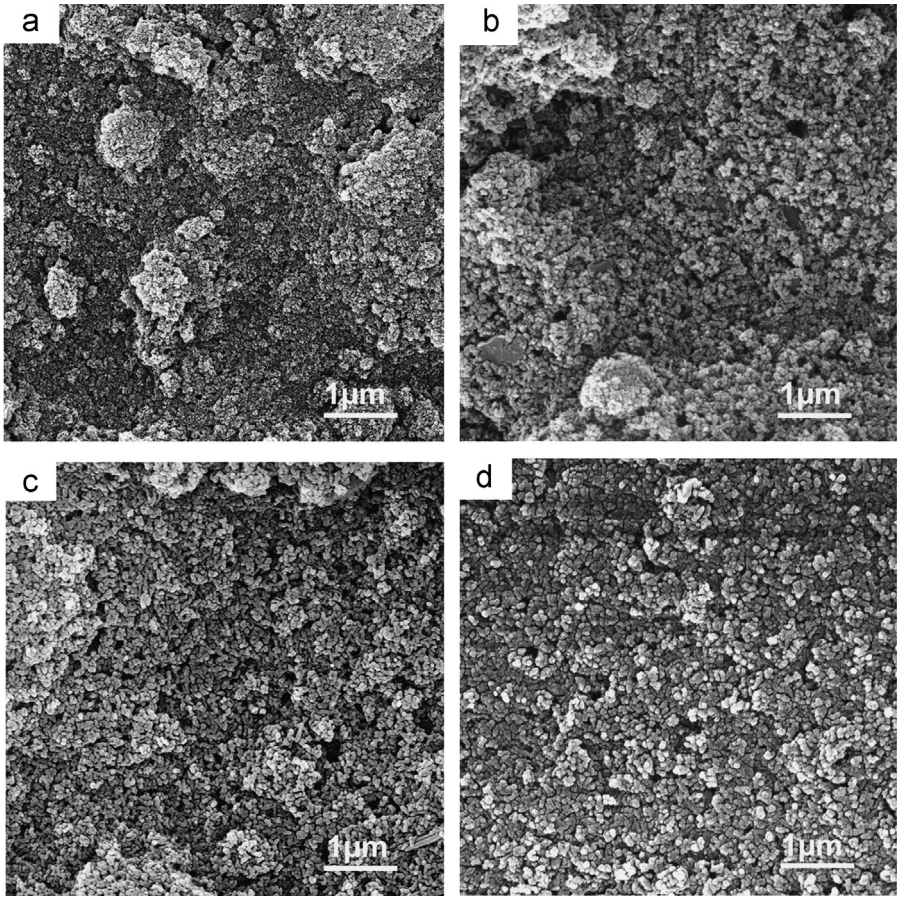

Fig. 7. High magnification SEM images of the unsintered coatings deposited at 20 V/cm and 60 s from (a) methanolic (b) ethanolic (c) isopropanolic and (d) butanolic suspensions.

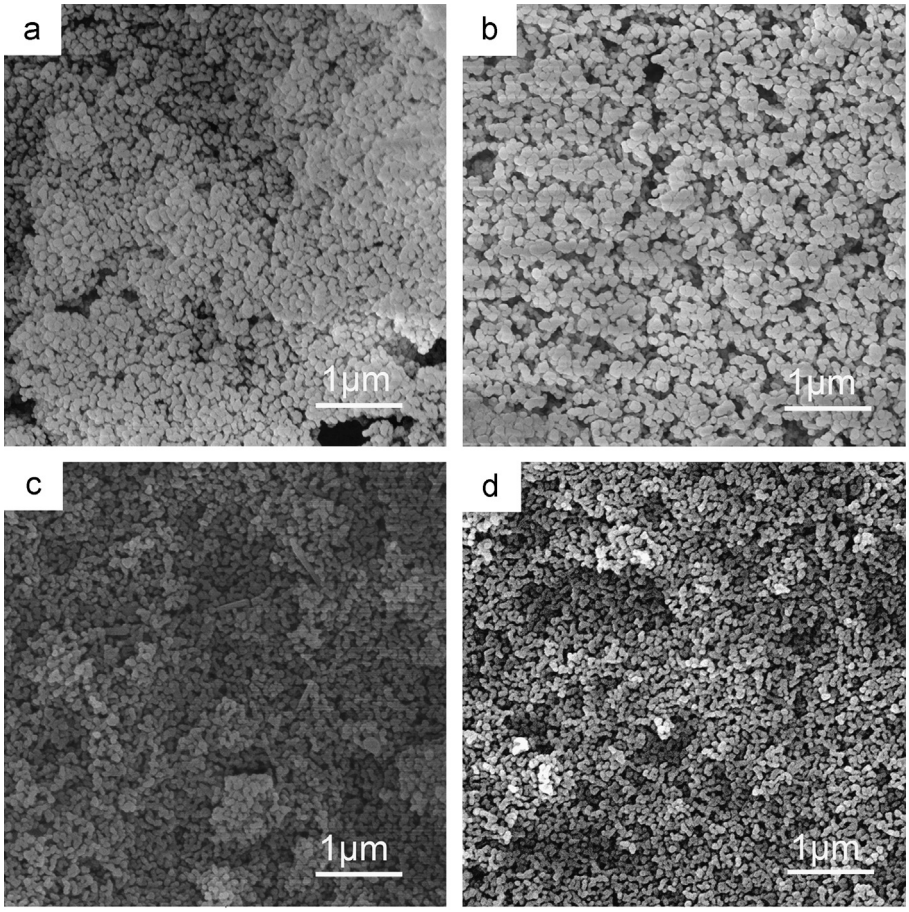

Fig. 8. High magnification SEM images of the sintered coatings deposited at 20 V/cm and 60 s from (a) methanolic (b) ethanolic (c) isopropanolic and (d) butanolic suspensions.

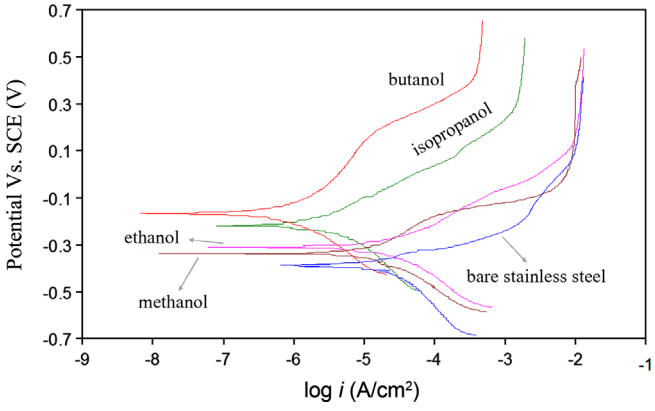

Fig. 9. The polarization curves for bare stainless steel substrate and HA coated substrates at 20 V/cm and 60 s from different alcoholic suspensions.

corrosion. The effect of EPD HA coatings on the corrosion resistance of the 316L stainless steel substrate in SBF solution has been investigated in several publications [9,29–31]. In these works isopropanol had been used as the medium for suspension preparation. X.F. Xiao and R.F. Liu [32] studied the stability of HA nanoparticles in different alcohols and found that the colloidal stability of HA is the highest in butanol so they selected butanol as the solvent for suspension preparation for HA EPD.

Table 2
The values of corrosion potential (E_{corr}) and current density (i_{corr}) extracted from polarization curves (Fig. 7).

Sample	E_{corr} (mV)	i_{corr} (μA/cm^2)
Bare stainless steel	−388	29.47
Methanolic	−338	27.62
Ethanolic	−312	21.66
Isopropanolic	−217	2.26
Butanolic	−168	0.584

The results obtained for microstructural analysis, adhesion strength and corrosion resistance of the coatings imply that butanol is the best suspension medium for HA EPD. The SEM microstructure of the coating deposited at 20 V/cm for 60 s from butanolic suspension and immersed for 1 week in SBF solution at 37.5 °C is shown in Fig. 10. It can be seen that the coating surface has been uniformly covered by apatite crystals after 1 week immersion in SBF solution at 37.5 °C. As it can be seen in SEM image (Fig. 10(a)) cracking occurs in the coating after immersion in SBF. These cracks are generated during drying the coating after taking it out from the SBF solution.

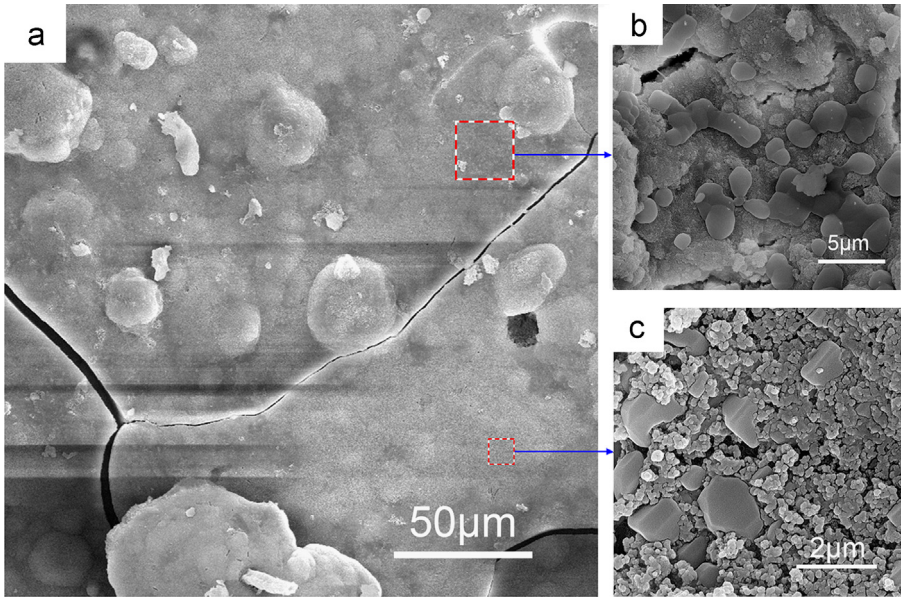

Fig. 10. SEM image of the coatings deposited at 20 V/cm for 60 s from butanolic suspension after its immersion in SBF solution for 1 week in different magnifications: (a)1 kx, (b) 20 kx and (c) 30 kx.

4. Conclusion

The suspensions of HA nanoparticles were prepared in different alcohols; it was found that $RCH_2OH_2^+$ species generated through alcohol ionization are adsorbed on the HA nanoparticles surface via hydrogen bonding with their P–OH surface group resulting in their positive zeta potential; also it was found that the zeta potential of HA nanoparticles increases as the molecular weight of alcohol increases due to the higher adsorption of $RCH_2OH_2^+$ species on particles surface. The kinetics of deposition was faster from the suspensions with small molecule size alcohols due to the higher electrophoretic mobility of HA nanoparticles in them. Among the coatings the one deposited from butanolic suspension had the finest microstructure without any cracks resulting in its highest corrosion protection efficiency. It was concluded that butanol is the best suspension medium for HA EPD. The surface of coatings deposited from butanolic suspension was covered by apatite crystals when they were immersed in SBF solution for 1 week proving their good bioactivity.

References

[1] T.S.B. Narasaraju, D.E. Phebe, Review: some physico-chemical aspects of hydroxylapatite, J. Mater. Sci. 31 (1996) 1–21.
[2] P. Ducheyne, L.L. Hench, A. Kagan II, M. Martens, A. Bursens, J.C. Mulier, Effect of hydroxyapatite impregnation on skeletal bonding of porous coated implants, J. Biomed. Mater. Res. 14 (1980) 225–237.
[3] L.L. Hench, Bioceramics, J. Am. Ceram. Soc. 81 (1998) 1705–1727.
[4] J.M. Gomez-Vega, E. Saiz, A.P. Tomsia, G.W. Marshall, S.J. Marshall, Bioactive glass coatings with hydroxyapatite and Bioglass® particles on Ti-based implants. 1. Processing, Biomaterials 21 (2000) 105–111.
[5] C.T. Kwok, P.K. Wong, F.T. Cheng, H.C. Man, Characterization and corrosion behavior of hydroxyapatite coatings on Ti6Al4V fabricated by electrophoretic deposition, Appl. Surf. Sci. 255 (2009) 6736–6744.
[6] X.F. Xiao, R.F. Liu, Effect of suspension stability on electrophoretic deposition of hydroxyapatite coatings, Mater. Lett. 60 (2006) 2627–2632.
[7] M. Wei, A.J. Ruys, B.K. Milthorpe, C.C. Sorrell, Solution ripening of hydroxyapatite nanoparticles: effects on electrophoretic deposition, J. Biomed. Mater. Res. 45 (1999) 11–19.
[8] M. Wei, A.J. Ruys, B.K. Milthorpe, C.C. Sorrell, J.H. Evans, Electrophoretic deposition of hydroxyapatite coatings on metal substrates: a nanoparticulate dual-coating approach, J. Sol–Gel Sci. Techn. 21 (2001) 39–48.
[9] M. Farrokhi-Rad, T. Shahrabi, Effect of triethanolamine on the electrophoretic deposition of hydroxyapatite nanoparticles in isopropanol, Ceram. Int. 39 (2013) 7007–7013.
[10] S. Kuche Loghmani, M. Farrokhi-Rad, T. Shahrabi, Effect of polyethylene glycol on the electrophoretic deposition of hydroxyapatite nanoparticles in isopropanol, Ceram. Int. 39 (2013) 7043–7051.
[11] L. Besra, M. Liu, A review on fundamental and applications of electrophoretic deposition, Prog. Mater. Sci. 52 (2007) 1–61.
[12] J. Ma, C. Wang, K.W. Peng, Electrophoretic deposition of porous hydroxyapatite scaffold, Biomaterials 24 (2003) 3505–3510.
[13] H.C. Hamaker, Formation of a deposit by electrophoresis, Trans. Faraday. Soc. 35 (1940) 279–287.
[14] M. von Smoluchowski, Versuch einer mathematischen theorie der Koagulationkinetik kolloider Loesungen,, Z. Phys. Chem. 92 (1917) 129–132.
[15] T. Uchikoshi, K. Ozawa, B.D. Hatton, Y. Sakka, Electrophoretic deposition of alumina suspension in a strong magnetic field, J. Mater. Res. 16 (2001) 321–324.
[16] M. Farrokhi-Rad, M. Ghorbani, Electrophoretic deposition of titania nanoparticles in different alcohols: kinetics of deposition, J. Am. Ceram. Soc. 94 (2011) 2354–2361.
[17] M. Farrokhi-Rad, T. Shahrabi, Electrophoretic deposition of titania nanoparticles: sticking parameter determination by an in-situ study of the EPD kinetics, J. Am. Ceram. Soc. 95 (2012) 3434–3440.
[18] M. Wei, A.J. Ruys, B.K. Milthorpe, C.C. Sorrell, Precipitation of hydroxyapatite nanoparticles: effects of precipitation method on electrophoretic deposition, J. Mater. Sci. Mater. Med. 16 (2005) 319–324.
[19] T. Kokubo, H. Takadama, How useful is SBF inpredicting in vivo bone bioactivity?, Biomaterials 27 (2006) 2907–2915
[20] R. Damodaran, B.M. Moudgil, Colloids Surf. A Physicochem. Eng. Aspects 80 (1993) 191–197.
[21] Ch. Reichardt, Appendix 8: Solvents for Acid/Base Titrations in Non-Aqueous Media, Solvent and Solvent Effects in Organic Chemistry, 3rd edition, Wiley-VCH, Weinheim, Germany, 2003, p. 496 (7).
[22] H.K. Varma, S.S. Babu, Synthesis of calcium phosphate bioceramics by citrate gel pyrolysis method, Ceram. Int. 31 (2005) 109–114.

[23] M. Kawata, H. Uchida, K. Itatani, I. Okada, S. Koda, M. Aizawa, Development of porous ceramics with well-controlled porosities and pore sizes from apatite fibers and their evaluations, J. Mater. Sci. Mater. Med. 15 (2004) 817–823.
[24] F. Miyaji, Y. Kono, Y. Suyama, Formation and structure of zinc-substituted calcium hydroxyapatite, Mater. Res. Bull. 40 (2005) 209–213.
[25] Z.H. Cheng, A. Yasukawa, K. Kandori, T. Ishikawa, FTIR study of adsorption of CO_2 on nonstoichiometric calcium hydroxyapatite, Langmuir 14 (1998) 6681–6686.
[26] T. Ishikawa, Surface structure and molecular adsorption of apatites, Stud. Surf. Sci. Catal. 99 (1996) 301–318.
[27] H. Tanaka, T. Watanabe, M. Chikazawa, FTIR and TPD studies on the adsorption of pyridine, n-butylamine and acetic acid on calcium hydroxyapatite, J. Chem. Soc. Faraday T Rans. 93 (1997) 4377–4381.
[28] I. Zhitomirsky, L. Gal-or, Electrophoretic deposition of hydroxyapatite, J. Mater. Sci.: Mater. Med 8 (1997) 213–219.
[29] N. Eliaz, M.T. Sridhar, U.Kamachi Mudali, Baldev Raj, Electrochemical and electrophoretic deposition of hydroxyapatite for orthopaedic applications, Surf. Eng. 21 (2005) 238–242.
[30] T.M. Sridhar, U. Kamachi Mudali, M. Subbaiyan, Preparation and characterization of electrophoretically deposited hydroxyapatite coatings on type 316L stainless steel, Corros. Sci. 45 (2003) 237–252.
[31] T.M. Sridhar, N. Eliaz, U.Kamachi Mudali, Baldev Raj, Electrophoretic deposition of hydroxyapatite coatings and corrosion aspects of metallic implants, Corros. Rev. 20 (2002) 255–293.
[32] X.F. Xiao, R.F. Liu, Effect of suspension stability on electrophoretic deposition of hydroxyapatite coatings, Mater. Lett. 60 (2006) 2627–2632.